Dynamic stall models for post flutter analysis of an aeroelastic wing section

Yann Blairon, Olivier Montagnier, Annie Leroy

DOI:

Dynamic stall models for post flutter analysis of an aeroelastic wing section

Yann Blairon†, Olivier Montagnier*, Annie Leroy**
** Research Center of French Air Force Academy (CREA)*
French Air Force Academy, F-13661 Salon-de-Provence, France
yann.blairon@ecole-air.fr – olivier.montagnier@ecole-air.fr – annie.leroy@ecole-air.fr
† Corresponding Author

Abstract

The design of solar HALE drones remains a major challenge for aircraft designers because of their design features of large span wings, necessarily very flexible, which are sensitive to external loads and subject to large displacements. They are thus susceptible to aeroelastic instabilities, which in turn tend to destabilize the drone in flight. For pre-design steps, in view of developing reliable tools that are founded on low order or medium fidelity full nonlinear approaches, this paper presents different dynamic stall models and an aeroelastic study to investigate stall flutter prediction on a two degree of freedom typical aeroelastic section. Three semi-empirical dynamic stall models chosen from the literature have been selected and implemented to investigate differences in their hypothesis, complexity, and performances to predict highly nonlinear aerodynamics. They were assessed by comparison with experimental data and test cases from the literature, in terms of aerodynamic coefficient prediction for an imposed pitch oscillation with different amplitude and reduced frequency and then, in terms of flutter critical airspeed and LCO prediction.

1. Introduction

HALE fixed-wing solar UAVs, such as NASA Helios and Airbus Zephyr prototypes, are among the innovative concepts for applications in the field of observation and telecommunications [1]. The design of such a solar UAV remains a major challenge for aircraft designers. Because such drones require a very good aerodynamic efficiency and a large surface area for solar panels to be fitted, most of the designs feature large span wings, which are necessarily very flexible, sensitive to external loads and subject to large displacements and rotations. They are thus susceptible to aeroelastic instabilities, which in turn tend to destabilize the drone in flight. The aeroelastic performance of this type of wing remains a scientific and technological challenge on which research efforts must still be carried out to improve its modelling and simulation combining structural dynamics, unsteady and nonlinear aerodynamics, and flight mechanics. Aeroelastic phenomena, i.e. flutter, are particularly a major concern for aircraft designers because of the dramatic consequences on the aircraft structure they can engender. For two decades now, several laboratories have endeavored to simulate and predict aeroelastic instabilities for such high flexible airplanes considering full nonlinear approaches [2-6]. Indeed, this kind of full aeroelastic modeling, being able to simulate the response of the structure to a gust for example, is required for pre-design phases of such wings and is more suitable than high fidelity numerical simulation tools due to their prohibitive computational costs.
Kirsch et al [6] led to the development of a computational code (GEBTAero) for the simulation of an anisotropic composite flexible wing allowing to determine the flutter critical airspeed for different configurations using aeroelastic tailoring. The model is based on a geometrically exact beam theory coupled with a two-dimensional unsteady finite state aerodynamic model. To date, as this model does not consider non-linear unsteady aerodynamics, such as dynamic stall that occurs for an airfoil during pitching and plunging oscillations, limit cycle oscillations (LCOs) that are observed in the neighbourhood of the flutter in wind tunnel experiments [2] cannot be predicted. Thus, to improve this predictive tool concerning aeroelastic modelling, this work focuses on one predominant issue to solve related to the aerodynamic dynamics of airfoils at high angles of attack. Using a typical 2D aeroelastic model of two degrees of freedom oscillating airfoil, combined to a dynamic stall model to compute aerodynamic forces and moments, the main

objective of this work is to implement different semi-empirical stall models to investigate their hypothesis, complexity and performances to predict highly nonlinear aerodynamics. The resulting nonlinear aeroelastic formulation can be solved in the frequency domain to predict the flutter critical airspeed and in the temporal domain to exhibit the airfoil movement and limit cycle oscillations that could be observed.
It is now well known that stall flutter was identified as a flutter type that airfoils could experience in rotorcraft systems in particular. Semi-empirical dynamic stall models such as Snel [7], Øye [8], ONERA [9] or the Beddoes-Leishman (B-L) [10] models, were developed to identify the correct aerodynamic loads and predict such behaviours. These models are still commonly used in the literature for aeronautical applications, as well as for aeroelasticity of wind turbine blades [11-13].
Regarding 2D aeroelastic modeling, in [14] and [15], numerical and experimental approaches are used to assess a semi-empirical model to predict flutter instability for a flate plate and a NACA 0012 airfoil respectively. In [14], LCOs amplitudes are given but not predicted. In [15], flutter occurrence and stable LCO have successfully been reproduced and predicted by the B-L model. These works offer the possibilities of using these results as test cases.

This paper is organised as follows: in section 2, aeroelastic equation of airfoil motion results are recalled. Three different models that have been selected for the comparison and shortly presented in section 3. Large pitch motions of a flat plate are studied with these models in section 4. Finally, preliminary results on flutter and LCO occurrence are presented and discussed in section 5 considering the test case studied in [13].

2. Aeroelastic equations of motion

The typical aeroelastic section is composed of an airfoil linked to a pitching spring and a plunge spring to simulate the two cinematic degrees of freedom. The motion is assumed positive downwards, with h representing the vertical plunging displacement, and the structural angle is defined by the value α while the aerodynamic angle of attack will be defined as $\theta = \alpha + \frac{\dot{h}}{U}$. This is the specific angle used when computing the aerodynamic loads for the airfoil. Figure 1 resumes the main parameters and values used to formulate the aeroelastic equations of motion.

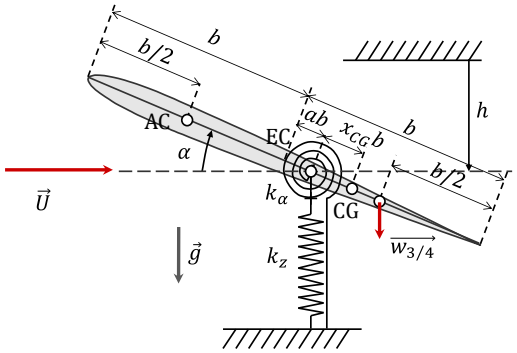

Figure 1: Two-dimensional aeroelastic model and main model parameters

The equations of motion can be expressed as follow:

$$m\ddot{h} + x_{CG}bm\ddot{\alpha} + c_h\dot{h} + k_h h = -L \tag{1}$$

$$J\ddot{\alpha} + x_{CG}bm\ddot{h} + c_\alpha\dot{\alpha} + k_\alpha\alpha + k_{NL}\alpha^3 = M \tag{2}$$

where m, J, b, x_{CG}, c_h, c_α, k_h, k_α and k_{NL} are the wing mass, the moment of inertia about the elastic centre (EC), the half-chord, the relative distance between EC and the centre of gravity (CG), the plunge and pitch viscous damping, the plunge and pitch stiffnesses, and the non-linear stiffness in pitch, respectively. The dot specifies the real time derivative. According to Theodorsen's theory [16] for low angles-of-attack, the unsteady lift and moment are written in the following form:

$$L = \pi s b^2 \rho\left[\ddot{h} + U\dot{\alpha} - ab\ddot{\alpha}\right] + s\rho b U^2 C_{L_\alpha} C(k)\left[\alpha_{3/4} - \alpha_0\right] \tag{3}$$

$$M = -\pi s b^3 \rho\left[\frac{1}{2}\ddot{h} + U\dot{\alpha} + b\left(\frac{1}{8} - \frac{a}{2}\right)\ddot{\alpha}\right] + b\left(\frac{1}{2} + a\right)L \tag{4}$$

with the angle-of-attack at collocation point (without linearisation)

$$\alpha_{3/4} = \alpha + \text{atan}\left(\frac{w_{3/4}}{U}\right) = \alpha + \text{atan}\left(\frac{\dot{h}}{U} + +b\left(\frac{1}{2} - a\right)\frac{\dot{\alpha}}{U}\cos\alpha\right) \quad (5)$$

where s, a, ρ, U and C_{L_α} are the span, the relative distance between EC and the airfoil centre, the air density, the fluid velocity and the lift coefficient derivative at zero lift, respectively. The complex Theodorsen's function $C(k)$ depends on the reduced frequency $k = \omega b/U$ which must be computed iteratively. Note that the first part of Eq. (3) and Eq. (4) corresponds to the non-circulatory terms, and the second part to the circulatory terms. In the following, the circulatory term in Eq. (3) will be replaced by the dynamic lift coefficient C_L^{dyn} and a set of ordinary differential equation (ODE) eliminating the iterative problem for solving the function $C(k)$.

3. Semi-empirical dynamic stall models

Dynamic stall is a nonlinear unsteady phenomenon that occurs when airfoils experience rapid angle of attack oscillations. Numerous papers can be found to explain main physical features encountered during this phenomenon exhibiting traveling vortices along airfoil surfaces and hysteresis cycle in lift generation. Dynamic stall models allow the computation of the resulting nonlinear aerodynamic loads during vortex shedding and displacement. These models are usually based on experimental data for the static lift curve of a specific airfoil and on state equations. These equations are used to achieve a delay between airfoil motion and lift onset, and consequently the hysteresis loop. Then, depending on the complexity of the model, various corrections can be made to take stall dynamics in account, and ODEs are formulated to model the time delay of the observed physics. Three different models have been selected form the literature for the comparison: Snel [7], Øye [8], and a modified B-L models [12,13]. This later is named "Risø model" in this paper. These models have been first developed for helicopter rotor blades or wind turbines applications. Nevertheless, by comparing fluid reduced time and reduced frequency calculated from 3 different typical datasets, Table 1 shows that these models remain relevant for HALE drone applications. Here $T_u = 2b/U$ is the time for the flow to travel a chord length.

Table 1: Typical values of fluid reduced time and reduced frequency (*data at mid-span)

			Helicopter Rotor [17]	**Wind Turbine [18]**	**HALE Drone [19]**
Wind speed	U	m/s	100*	34*	55
Chord length	c	m	0.5*	2*	2
Fluid reduced time	T_u	s	0.025	0.029	0.018
Structural frequency	$\omega/2\pi$	Hz	5	0.2	1
Reduced frequency	k	-	0.08	0.04	0.11

The three models are briefly presented in the following subsections. More details can be found in the corresponding references.

2.1 Snel Model

The Snel model is a second-order dynamic stall model that uses no airfoil specific adjustment settings in its formulation but can nevertheless predict dynamic stall as models that do require such input. As exposed in [7] or [20], the model is based on the difference between the dynamic and steady lift coefficient than can be written as:

$$C_L^{dyn} = C_L^{st} + \Delta C_{L,1} + \Delta C_{L,2} \quad (6)$$

The first correction term describes the forcing frequency response and the second one is added to estimate the higher frequency dynamics of a self-excited nature such as vortex shedding. In this study, only the first order correction term will be considered. To compute the forcing frequency response, it's required to use the following ODE:

$$\Delta\dot{C}_{L,1} + \frac{c_{10}}{T_u}\Delta C_{L,1} = \Delta\dot{C}_L^{att} \tag{7}$$

where ΔC_L^{att} is the difference between the potential flow lift and the steady lift. It can be seen as a switch between the attached flow and the stalled flow regimes as it will be close to zero before stall and then start affecting the system of equations after stall. c_{10} can be seen as the spring stiffness for the ODE system and is obtained given the expression of the airfoil plunge movement:

$$c_{10} = \begin{cases} \dfrac{1 + 0.5\Delta C_L^{att}}{8 + 640T_u\dot{\alpha}} & if \quad \dot{\alpha}C_L^{att} > 0 \\ \dfrac{1 + 0.5\Delta C_L^{att}}{8 - 480T_u\dot{\alpha}} & if \quad \dot{\alpha}C_L^{att} \leq 0 \end{cases} \tag{8}$$

In this model, only the dynamic lift coefficient is considered. Static drag and moment coefficients are not modified.

2.2 Øye Model

The Øye model [8] is a quite simple dynamic stall model that uses a single first order ODE to simulate the time delay of the lift response to the variations in the angle of attack. It introduces a variable *f*, called the interpolation factor, to model the relative importance of two physics which represent a fully attached regime and a fully separated one. It is then necessary to have two corresponding curves. The main hypothesis of the model is that the fully separated lift coefficient C_L^{fs} is an Hermite polynomial verifying empirical conditions ($C_L^{fs}\big|_{\alpha_0} = 0$, $C_L^{fs}\big|_{\alpha_{fs}} = C_L^{st}|_{\alpha_{fs}}$, $C_L^{fs\prime}\big|_{\alpha_0} = C_L^{st\prime}|_{\alpha_0}/2$, $C_L^{fs\prime}\big|_{\alpha_{fs}} = C_L^{st}|_{\alpha_{fs}}/12$) and the static lift experimental (or numerical) curve C_L^{st} is weighted between the attached flow and the fully separated flow via the relative position of the separation point in static f_{st} (see Figure 2):

$$C_L^{st} = f_{st}C_L^{att}(\alpha) + (1 - f_{st})C_L^{fs}(\alpha) \tag{9}$$

Rewriting this equation allows to compute the separation point function:

$$f_{st} = \frac{C_L^{st} - C_L^{fs}}{C_L^{att} - C_L^{fs}} \quad \text{with} \quad C_L^{att} = C_{L_\alpha}(\alpha - \alpha_0) \tag{10}$$

where C_L^{att} is the fully attached lift coefficient. Note that $f_{st} = 1$ for a fully attached flow and $f_{st} = 0$ for a fully detached flow. The state equation of the model assumes a lag between the static and the dynamic separation point positions:

$$\dot{f}_{dyn} + \frac{1}{T_f}f_{dyn} = \frac{1}{T_f}f_{st} \tag{11}$$

where $T_f = \tau_f T_u$ is a characteristic time determined numerically or experimentally. The dynamic lift is then obtained:

$$C_L^{dyn} = f_{dyn}C_L^{att}(\alpha) + \big(1 - f_{dyn}\big)C_L^{fs}(\alpha) \tag{12}$$

As Snel model, only the dynamic lift coefficient is considered. Static drag and moment coefficients are not modified.

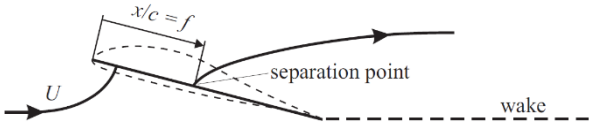

Figure 2: Separation point definition on a flat plate [13]

2.3 Risø Model

The Risø model [12-13] is a modified Beddoes-Leishmann dynamic stall model. The main difference is that the possible leading-edge separation point has been neglected. It is not a dominant phenomenon for relative airfoil

thicknesses of less than 15%, as in the case of wind turbine application for which the model was originally developed. The approach is similar to that of Øye, but numerous effects have been added.
The first part of the Risø model correspond to the unsteady attached flow (circulatory term in Eq. (3)). In order to replace Theodorsen's theory, the angle of attack at collocation point is replace with an effective angle of attack:

$$\alpha_E = \alpha_{3/4}\,(1 - \mathrm{A1} - \mathrm{A2}) + x_1 + x_2 \tag{13}$$

where x_i are state variable of the fluid and A_i are constants obtained numerically or experimentally. These two state variables that represent the downwash time lag, are obtained using the following state equations:

$$\dot{x_i} + U\frac{b_i}{b}x_i = U\frac{b_i A_i}{b}\alpha \qquad \forall i \in \{1,2\} \tag{14}$$

where b_i are new constants. This effective angle of attack allows to compute the unsteady attached lift coefficient:

$$C_L^{att} = C_{L_\alpha}(\alpha_E - \alpha_0) + \pi\frac{b\dot{\alpha}}{U} \tag{15}$$

The second part correspond to the trailing edge (TE) separation. The basic assumption is that the static curve can be represented by the expression:

$$C_L^{st} = C_{L_\alpha}\left(\frac{1+\sqrt{f_{st}}}{2}\right)^2(\alpha - \alpha_0) \tag{16}$$

The inversion of the previous equation directly gives the expression of f_{st} (see [13]). The logic is reversed with respect to the Øye model, since equation (9) is used to calculate the totally separate lift coefficient.

$$C_L^{fs}(\alpha) = \frac{C_L^{st} - C_{L_\alpha}(\alpha - \alpha_0)f_{st}(\alpha)}{1 - f_{st}} \tag{17}$$

The dynamic of the separation is given with two other state variables equation. The first one representing the dynamic of the TE separation and assume a delay between pressure and airfoil lift:

$$\dot{x_3} + \frac{1}{T_p}x_3 = \frac{1}{T_p}C_L^{att} \tag{18}$$

where $T_p = \tau_p T_u$ is the characteristic lag time between pressure and lift. The state x_3 can be assimilated to a lag lift and can be noted $x_3 = C_L^{p'}$. It can be deduced a new angle of attack for that lift coefficient:

$$\alpha_f = \frac{C_L^{p'}}{C_{L_\alpha}} + \alpha_0 \tag{19}$$

The last state equation is similar to Eq. (8) and gives the dynamic of the separation point:

$$\dot{x_4} + \frac{1}{T_f}x_4 = \frac{1}{T_f}\,f_{lag} \qquad \text{where } f_{lag} = f_{st}(\alpha_f) \tag{20}$$

This new state x_4 is denoted f_{dyn}. Finally, the dynamic lift coefficient can then be computed:

$$C_l^{dyn} = C_{L_\alpha}(\alpha_E - \alpha_0)f_{dyn} + C_L^{fs}(\alpha_E)\left(1 - f_{dyn}\right) + \pi\frac{b\dot{\alpha}}{U} \tag{21}$$

Risø model proposes also to estimate the dynamic drag and moment coefficients as:

$$C_D^{dyn} = C_D^{st}(\alpha_E) + (\alpha - \alpha_E)C_L^{dyn} + \frac{1}{4}\left(C_D^{st}(\alpha_E) - C_{D_0}\right)\left(\left(1 - \sqrt{f_{dyn}}\right)^2 - \left(1 - \sqrt{f_{st}(\alpha_E)}\right)^2\right) \tag{22}$$

$$C_M^{dyn} = C_M^{st}(\alpha_E) + C_l^{dyn}\left(a^{st}(f_{dyn}) - a^{st}(f_{st}(\alpha_E))\right) - \pi\frac{b\dot{\alpha}}{2U} \quad (23)$$

with a^{st} the position of an equivalent pressure center defined by the static lift and moment curves as $a^{st}(\mathrm{f}) = \left(C_M^{st} - C_{M_0}^{st}\right)/C_L^{st}$.

4. Results

4.1 Comparison of dynamic stall models in case of a pitch oscillation

All dynamic stall models are implemented in Matlab using ode45 function. In this first step, it is proposed to compare the models for a prescribed motion case before conducting aeroelastic simulations. Hofmann et al. [21] performed several pitch motions on wind turbine airfoils. For example, the experimental case of a NACA 4415 at $k = 0.023$, $\alpha_{mean} = 14°$ and $\alpha_{amp} = 10.5°$ is presented in Figure 3. The three models presented here are plotted. For comparison, Holierhoek simulations for the B-L and ONERA models are also shown [20]. Two phases can be distinguished during the angle of attack growth. In the first, up to around 12 degrees, all the models are close to the experimental curve, the best being the ONERA model. At 14 degrees, the experimental curve reaches the maximum lift corresponding to the instant of leading-edge vortex convection [17]. This extra lift is only well captured by the B-L model and, to a lesser extent, by the Snel and ONERA models. In the second phase up to the nominal angle, all models except ONERA's follow the same slope. The slope of the ONERA model is steeper and resembles the experimental curve, even if it remains the model most distant from the experimental values. As the angle of attack decreases, the behaviour of the models is very similar except at the smallest angles, where the gap increases. Overall, the models are close to the experimental curve in this phase.

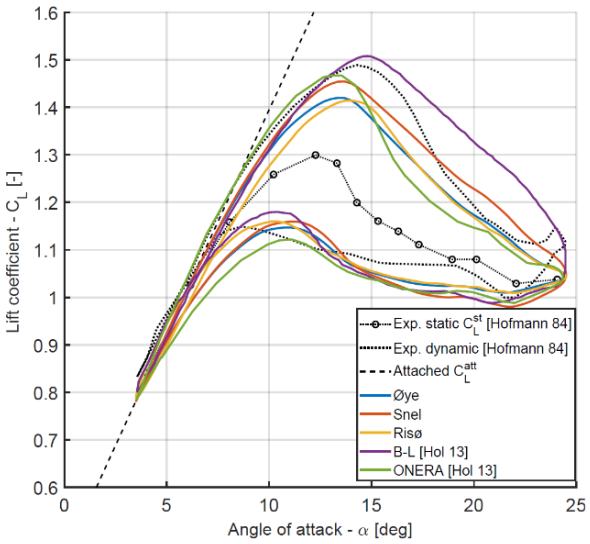

Figure 3: Dynamic stall models on the NACA 4415 airfoil for $k = 0.023$ ($\alpha_{mean} = 14°$ and $\alpha_{amp} = 10.5°$)

4.2 Dynamic stall of a flat plate in sinusoidal pitch motion

The aeroelastic study of the final section involves a flat plate. In this section, sinusoidal pitch motion is investigated on a flat plate at a reduced frequency ($k = 0.1$) close to the aeroelastic case ($k \approx 0.08$).
Figure 4 illustrates the pitch oscillations of ±4° around the aerodynamic centre for mean angles of 5°, 10°, and 15°. Figure 4a and 4b display the lift coefficients for the Oye and Riso models, respectively. For these simulations, the static curve (C_L^{st}) is obtained from Amandolese et al [14]. In these figures, the C_L^{fs} and f_{st} functions are plotted, and they differ slightly between the two models. For small angles of attack oscillations (black curve), it is noteworthy that the Oye model does not exhibit any unsteady effect. This is not the case for the Riso model, due to the state equations (14). For oscillations around 10 and 15 degrees (blue and green curves), the behaviour of the two models is quite similar. This is attributed to the use of the same τ_f in equations (11) and (20) (see Table 2). However, it should be

noted that the hysteresis loops are more significant for the Oye model. The dynamic drag and quarter chord moment are not considered for the Oye model. Figure 4c shows the Riso model drag, with static curve coming from Fage et al. [22]. The effect of dynamic stall is very weak. Finally, Figure 4d shows the quarter-chord moment coefficient. Due to the lack of data on the moment coefficient for the flat plate at high angle of attack, the static curves are obtained from [23] until 20 degrees, and data from the NACA0009 airfoil at higher angle of attack are used [24]. The effect of dynamic stall is more significant in this case, reaching approximately a 50% deviation from the static value at 10° (blue curve).

Table 2: Non-dimensional parameters of the models

τ_f	τ_p	A_1	b_1	A_2	b_2
6	1.5	0.165	0.0455	0.335	0.3

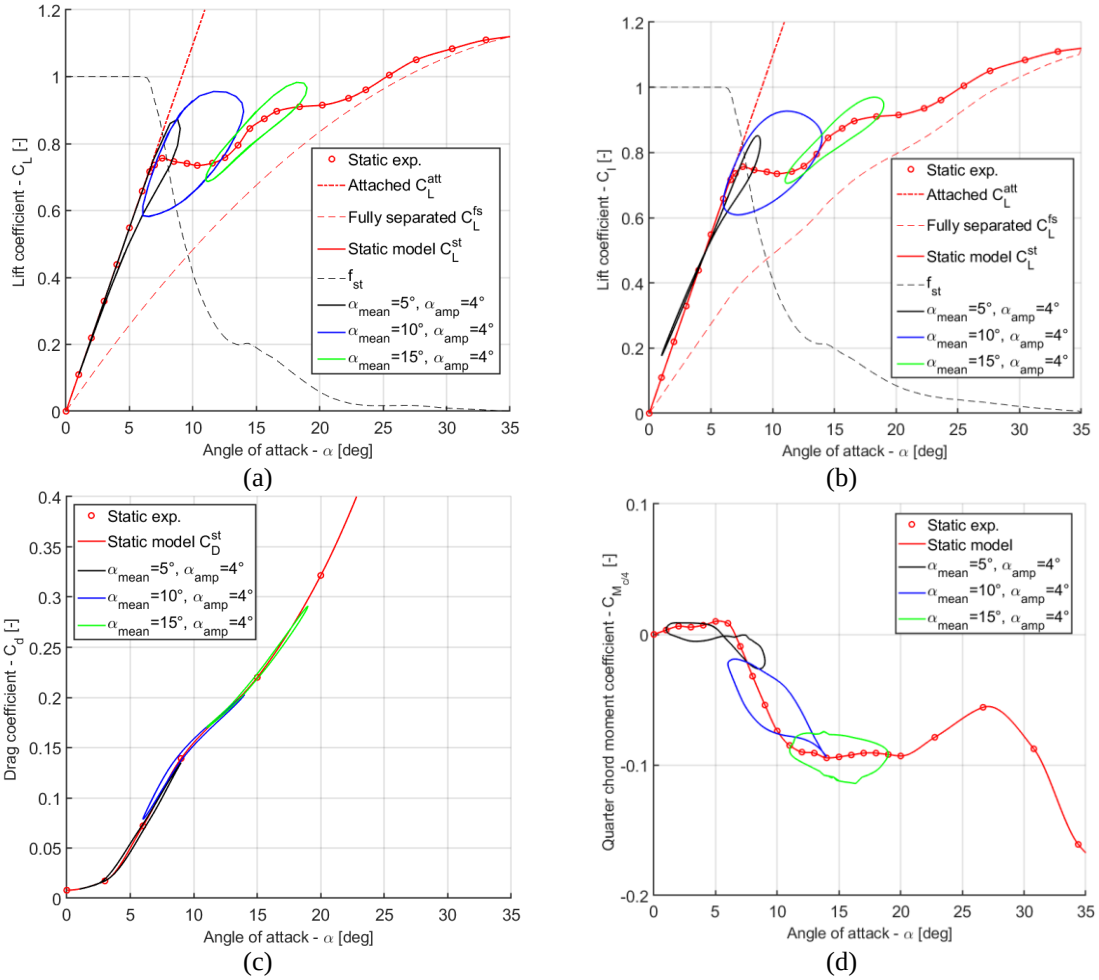

Figure 4: Dynamic stall simulations for various sinusoidal pitch oscillations ($\alpha_{mean} \in \{5°, 10°, 15°\}$ and $\alpha_{amp} = 4°$): (a) lift coefficient for Øye model; (b), (c), & (d), lift, drag and quarter chord moment for Risø model

Figure 5 depicts the pitch motion of the wing at zero mean angle and amplitudes of $\pm 10°$, $\pm 20°$ and $\pm 30°$, which are much more representative of aeroelastic limit cycles. Like the previous case, the dynamic lift between the Oye and Riso models remains relatively close during the angle of attack growth. However, the models diverge further during the descent phase. In the extreme case (green curve), the lift coefficient can reach 1.5, whereas the static value at 25° is approximately 1. The drag is still minimally affected by the Riso model. Conversely, the effect on the moment is very significant. In the extreme case (green curve), the coefficient reaches ±0.8, whereas it is zero in the static case. These calculations show that dynamic moment cannot be neglected in aeroelastic simulations, whereas the effect on drag can be.

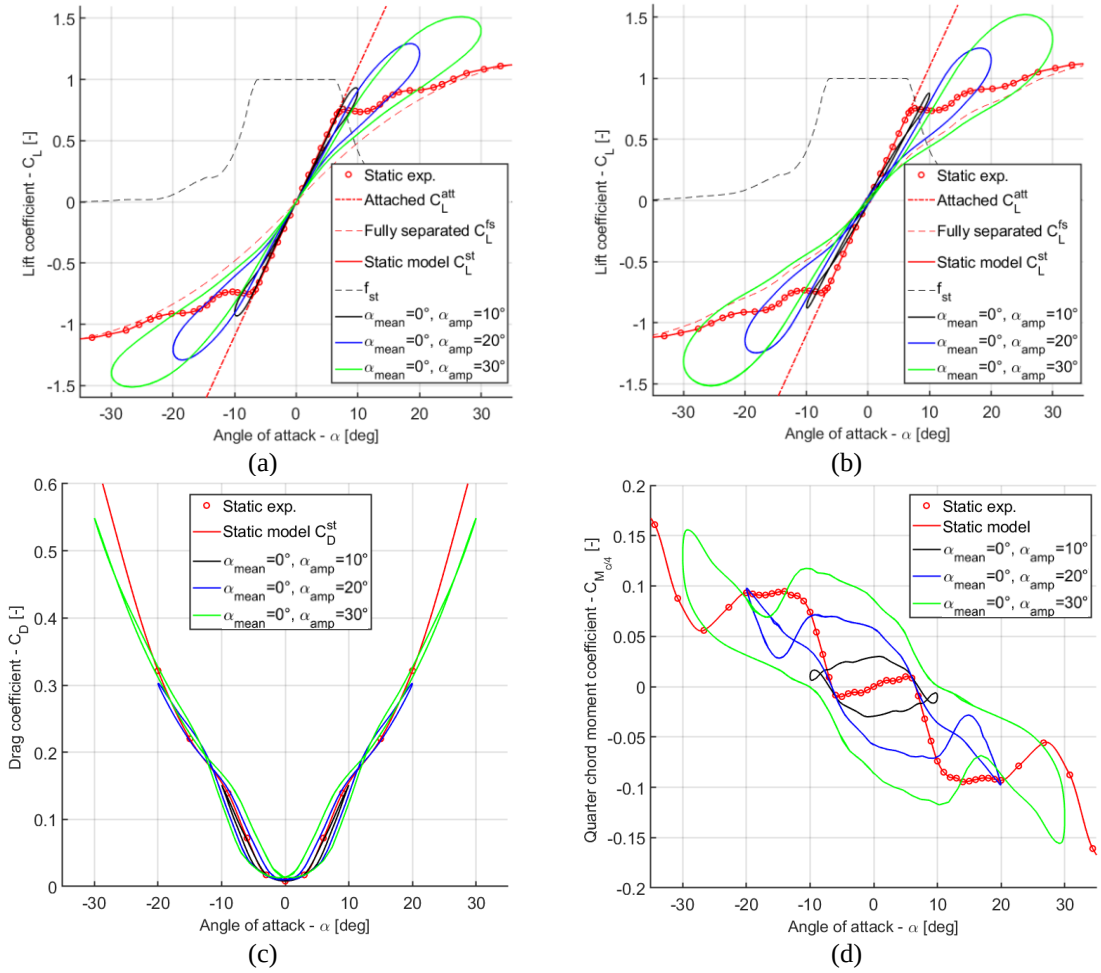

Figure 5: Dynamic stall simulations for various sinusoidal pitch oscillations ($\alpha_{mean} = 0°$ and $\alpha_{amp} \in \{10°, 20°, 30°\}$): (a) lift coefficient for Øye model; (b), (c), & (d), lift, drag and quarter chord moment for Risø model

4.3 Aeroelastic computations

Aeroelastic models using space-state formulation have been implemented in the Matcont toolbox in Matlab. The experimental case studied is that of the flat plate proposed by Amandolese et al. [14]. The data for equations (1-4) are fully defined in [14]. In the paper, the authors identified a cubic softening nonlinearity on the torsional stiffness, which is accounted for in all the models studied here. Figures 6a and 6b present the amplitude of the experimental limit cycles in pitch and plunge respectively, as a function of the dimensionless speed with respect to the flutter speed. The blue curves correspond to the increasing speed phase, while the red curves correspond to the decreasing speed phase from the stable limit cycles. A significant hysteresis is observed between the instability onset speed and the return to the initial equilibrium state. This phenomenon is characteristic of a subcritical bifurcation.
First, two aerodynamic models without dynamic stall are plotted. The first one is the pseudo-static model (equations (3-5) with C(k)=1), and the second one corresponds to the attached unsteady Riso model (Eq (14) only) referred to as Theodorsen in the figure. Note that the geometric nonlinearities of equation (5) are preserved. Both models exhibit subcritical bifurcations, but the amplitude of the limit cycles is not representative of the experiments at all. This indicates that the nonlinear torsional stiffness alone cannot explain the amplitude of the limit cycles in this experiment. The Oye and Riso models, assuming zero drag and quarter-chord moment, as well as the complete Riso model, are plotted. All three models exhibit subcritical bifurcations, but the amplitudes are lower than the experimental results. The bifurcation diagram of the Oye model shows a relatively similar shape, while the Riso model exhibits higher amplitudes that are closer to the real case. In particular, it is noteworthy that the prediction is improved by taking the drag and the quarter-chord moment in account. These results are preliminary, and in the future, the discrepancy between the models and the experiments will be further investigated. In particular, the B-L model, which exhibits higher dynamic coefficients (Figure 3), could be investigated.

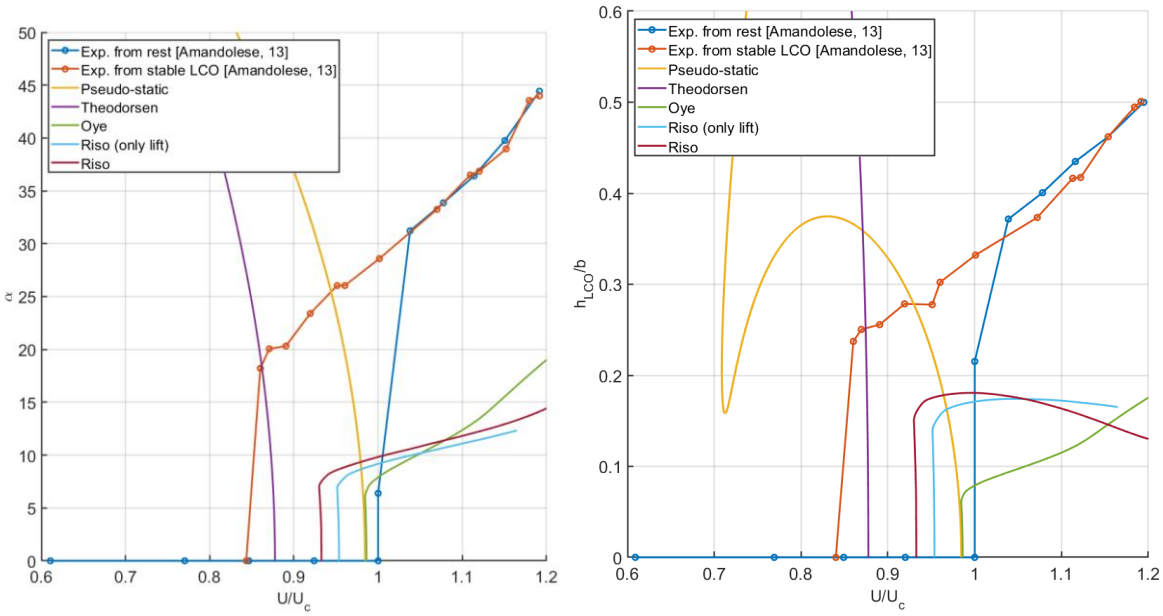

(a) (b)

Figure 6: Bifurcation diagram of the Amandolese *et al.* [14] case for various models: (a) pitch motion; (b) plunge motion.

5. Conclusion and perspectives

Aeroelastic motion equations for an airfoil were combined with semi-empirical dynamic stall models chosen from the literature that have been selected and implemented to investigate differences in their hypothesis, complexity, and performances to predict highly nonlinear aerodynamics. Results were assessed by comparison with experimental data and test cases from the literature, in terms of aerodynamic coefficient prediction for an imposed pitch oscillation with different amplitude and reduced frequency and then, in terms of flutter critical airspeed and LCO prediction for different flow velocities.

The test case of the dynamic response of a two-degree of freedom flat plate section undergoing flutter was discussed especially in this paper. Dynamic effects on the drag coefficient can be seen as negligeable for any range of motion, while the dynamic effect on moment coefficient and lift coefficient are seen to be heavily impacted for high amplitudes of pitch motion. When studying the different dynamic models and their impact on the stability analysis performed with Matcont toolbox in Matlab, we can observe that the flutter onset critical speed is slightly different according to the different dynamic stall models whereas the appearance of the LCOs is similar.

Future work will be dedicated to implement other and evolving dynamic stall models, and to perform a parametric study to investigate additional reduced frequency and angle of attack ranges. It will bring new results to highlight the capability and the differences between these dynamic stall models to predict flutter onset speed and stable LCOs.

6. Acknowledgments

This work is conducted in the framework of a PHD position at the French Air Force Academy and is supported in part by a grant of the French government defence agency DGA-AID (https://www.defense.gouv.fr/aid/appels-a-projets/appel-a-projets-theses-aid-classiques) and by the French Air Force Academy.

7. References

[1] Cestino E. 2006. Design of solar high altitude long endurance aircraft for multi payload & operations. *Aerospace science and technology*. 10 (6), 541-550.

[2] Patil M.J. & Hodges D.H. 2006. Flight dynamics of highly flexible flying wings. *J Aircraft*. 43 (6), 1790–1799.

[3] Shearer C.M. & Cesnik C.E. 2007. Nonlinear flight dynamics of very flexible aircraft. *J Aircraft*, 44 (5), 1528–1545.
[4] Del Carre A. et al. 2019. SHARPy: A dynamic aeroelastic simulation toolbox for very flexible aircraft and wind turbines. *J Open Source Softw*, 4 (44), 1885.
[5] Ribeiro F.L.C. et al. 2012. Aeroflex: a toolbox for studying the flight dynamics of highly flexible airplanes. In: VII CNEM. Brasil.
[6] Kirsch B., Montagnier O., Bénard E. & Faure T. 2020. Tightly coupled aeroelastic model implementation dedicated to fast aeroelastic tailoring optimisation of high aspect ratio composite wing. *J Fluids Struct*, 94, 102930.
[7] Snel, H. 1997. Heuristic modelling of dynamic stall characteristics. In EWEC-CONFERENCE. Bookshop for Scientific Publications. 429-433.
[8] Øye, S. 1991. Dynamic stall simulated as time lag of separation. In *Proceedings of the 4th IEA Symposium on the Aerodynamics of Wind Turbines*, Rome, Italy. 27, p28.
[9] Petot D. 1989. Differential equation modelling of dynamic stall. *La recherche aérospatiale* (English Edition). 5 : 59-72.
[10] Leishman, J. G., & Beddoes, T. S. 1989. A Semi-Empirical model for dynamic stall. *J of the American Helicopter society*, 34(3), 3-17.
[11] Larsen J.W., Nielsen S.R.K. and Krenk S. 2007. Dynamic stall model for wind turbine airfoils. *J Fluids and Structures*. 23, 959-982.
[12] Hansen, M. H. 2004. Aeroelastic stability analysis of wind turbines using an eigenvalue approach. Wind Energy: *An Int. J for Progress and Applications in Wind Power Conversion Technology*, 7(2), 133-143.
[13] Hansen, M. H., Gaunaa, M., & Madsen, H. A. 2004. A Beddoes-Leishman type dynamic stall model in state-space and indicial formulations. Denmark. Forskningscenter Risoe. Risoe-R No. 1354(EN)
[14] Amandolese, X., Michelin, S., & Choquel, M. 2013. Low speed flutter and limit cycle oscillations of a two-degree-of-freedom flat plate in a wind tunnel. *J Fluids Struct*, 43, 244-255.
[15] dos Santos, C. R., Pereira, D. A., & Marques, F. D. 2017. On limit cycle oscillations of typical aeroelastic section with different preset angles of incidence at low airspeeds. *J Fluids Struct*, 74, 19-34.
[16] Theodorsen, T. 1935. General theory of aerodynamic instability and the mechanism of flutter. Annual Report of the National Advisory Committee for Aeronautics, 268, 413.
[17] Leishman, G. J. 2006. Principles of helicopter aerodynamics. Cambridge university press.
[18] Arany, L., Bhattacharya, S., Macdonald, J., & Hogan, S. J. (2015). Simplified critical mudline bending moment spectra of offshore wind turbine support structures. *Wind Energy*, 18(12), 2171-2197.
[19] Lei, P., Lv, B., Guo, H., Kou, X., & Yu, L. 2019. Research on the Influences of Inertial Properties on Body Freedom Flutter for an Airfoil. In Journal of Physics: Conference Series (Vol. 1300, No. 1, p. 012087). IOP Publishing.
[20] Holierhoek, J. G., De Vaal, J. B., Van Zuijlen, A. H., & Bijl, H. 2013. Comparing different dynamic stall models. *Wind Energy*, 16(1), 139-158.
[21] Hoffman, M. J., R. R Ramsay and G. M. Gregorek. 1994. Unsteady aerodynamic performance of wind turbine airfoils, In: *AWEA Wind Power 94 Conference*, Mineapolis.
[22] Fage, A., & Johansen, F. C. 1927. On the flow of air behind an inclined flat plate of infinite span. Proceedings of the Royal Society of London. Series A, Containing Papers of a Mathematical and Physical Character, 116(773), 170-197.
[23] Pelletier, A., & Mueller, T. J. 2000. Low Reynolds number aerodynamics of low-aspect-ratio, thin/flat/cambered-plate wings. *Journal of aircraft*, 37(5), 825-832.
[24] Sheldahl, R. E., & Klimas, P. C. 1981. Aerodynamic characteristics of seven symmetrical airfoil sections through 180-degree angle of attack for use in aerodynamic analysis of vertical axis wind turbines (No. SAND-80-2114). Sandia National Labs., Albuquerque, NM (USA).